On the transversely isotropic, hyperelastic response of CNS white matter using a hybrid approach

Yi Pan¹, David Shreiber², and Assimina A. Pelegri ^{1,*}

¹Rutgers, the State University of New Jersey, Mechanical and Aerospace Engineering

98 Brett Road, Piscataway, NJ 08854

²Rutgers, the State University of New Jersey, Biomedical Engineering 599 Tailor Road, Piscataway, NJ 08854

Abstract

A numerical and experimental hybrid approach is developed to study the constitutive behavior of the central nervous system white matter. A published transversely isotropic hyperelastic strain energy function is reviewed and used to determine stress-strain relationships for three idealized, simple loading scenarios. The proposed constitutive model is simplified to a three-parameter hyperelastic model by assuming the white matter's incompressibility. Due to a lack of experimental data in all three loading scenarios, a finite element model that accounts for micro-structural axons and their kinematics is developed to simulate behaviors in simple shear loading scenarios to

^{*} Corresponding Author, email: pelegri@rutgers.edu

supplement existing uniaxial tensile test data. The parameters of the transversely isotropic hyperelastic material model are determined regressively using the hybrid data. The results highlight that a hybrid numerical virtual test coupled with experimental data, can determine the transversely isotropic hyperelastic model. Besides, it is noted that the model is not limited to small strains, but it is also applied to large deformations.

1. Introduction

The study of injury to the central nervous system (CNS), including brain and spinal cord, has been of great interest in recent years (Arbogast 1999, Meaney 2003, Bain 2003, Faul 2010, Amstrong 2015, Carlsen 2015, Goriely 2015). Traumatic brain injury (TBI) is often a consequence of blunt impact in sports, falls, motor vehicle crashes, and explosive blast shock waves. Spinal cord injury (SCI) also can occur in these trauma settings. Axonal injury, which is considered to be a significant contributor to cognitive dysfunction following TBI and functional deficits following SCI, represents a critical focal area for injury prevention and treatment, according to Amstrong 2015. Prevention of axonal injury in TBI and SCI requires knowledge of the external force transfer mechanisms from the head or torso to the axon level, which occurs at multiple length scales, thus increasing the problem complexity. Of the various mechanical parameters, the strain has been proposed as a reliable predictor of axonal injury (Meaney 2003); thus, accurate strain prediction depends on reliable mechanical behavior models and high fidelity anisotropic structural models (Carlsen 2015). Although finite element methods have been applied to predict the strain within the CNS white matter, they generally fail to capture the axon-level strains of the structural injury. The latter is partially due to the selection of the constitutive models that treat the material as homogeneous, ignoring the fundamental differences between the axons' mechanical properties and those of the extracellular matrix (ECM). In some studies, CNS white matter was modeled as a hyperelastic material using various hyperelastic models such as Ogden's, Mooney-Rivlin's, or Fung's, or even Neo-Hookean ones. The parameters of the models have been fitted in many experimental studies, with some representative ones found in Rashid 2012a, 2012b, and 2014. However, more work needs to be accomplished to address the anisotropy in Young's and shear modul observed in the brain tissue, starting from animal models that have been already highlighted in the literature including porcine brain (Arbogast, 1999), lamb brain (Feng 2013), and ovine brain (Labus 2016).

CNS white matter has been treated as an anisotropic, orthotropic, or transversely isotropic composite material by considering the long axons as reinforcing fibers embedded in an isotropic extracellular matrix (ECM). Previous studies have indicated that axons interact with the glial matrix through myelin, which is an insulating sheath made by oligodendrocytes (a particular type of neuroglia that supports and insulates axons) that, in addition to improving the speed of electrical conduction along the axon, also serves to interconnect axons (Arbogast 1999, Meaney 2003) physically. As a result, the mechanical behavior of white matter can be generally described with a transversely isotropic hyperelastic model, which has been supported by experimental characterization (Feng 2013, Giordano 2014, Labus 2016). The complexity of these constitutive models increases the difficulty of performing the necessary experiments to generate the required data and data reduction methods to determine the material parameters. Inverse procedures have been applied to recover material parameters from the results of finite element models (Miller 2000, Ho 2007, Rashid 2012b, Feng 2013, Javid 2014).

Most of these studies have assumed that the reinforcing axons in the composite are perfectly connected to its surrounding matrix treated as a homogeneous matrix material, and

therefore the axons follow idealized affine behavior. However, evidence has shown that the undulated axons demonstrate significant non-affine behavior, especially at low stretch levels. As tissue-level strain is increased, axons are increasingly recruited by the matrix and transition to affine behavior as they are being stretched (Bain 2003, Hao 2007). This transitional coupling between the axons and the matrix dictated, in part, by myelin, occurs through the nodes of Ranvier. Since it is known that axons are most sensitive to tension, incorporating the microscale transitional behavior from non-affine to affine mechanics and the dependence of this transition on myelin are critical steps towards accurately describing the axon-level strain that results the from tissue-level deformation. We have previously incorporated discrete transitions into a finite element model to study the mechanical response of white matter and simulate its structural fidelity (Pan 2011, 2013). However, this approach has a heavy computational burden and significantly increases the modeling complexity.

Feng and colleagues proposed a new strain energy density function capable of capturing the anisotropy of fiber composites in both shear and tension with respect to the fiber axis (Feng 2013). Besides an in-plane shear modulus μ and a parameter ζ that captures the difference of the Young's moduli in two different principal directions, a third parameter ϕ was introduced to include the shear anisotropy in the framework of hyperelasticity. Their model was further simplified to a transversely linear elastic compliance matrix in the small strain regime, which was applied to characterize the material properties of the corpus callosum of lamb brain. Although the fibermatrix interaction is highlighted by the parameter ϕ , the hyperelastic model was not advanced to represent the transitional coupling of matrix and undulated fibers, particularly at large strains.

In the current work, the hyperelastic material model in (Feng 2013) is applied to characterize the mechanical behavior of the white matter of chick embryo spinal cord beyond the linear elastic range. Instead of using the simplified small strain elastic model, the stress response under simple in-plane shear, out-of-plane shear, and uniaxial tensile loading conditions were derived from the regime's constitutive model of large deformation. The three independent material parameters of the incompressible model were obtained by combining curve fitting of experimental data with finite element simulations of idealized behavior in other mechanical testing modes using our previously developed model (Pan 2011, 2013). This FE model captures the tortuous microstructure of axons and the kinematics of undulated axons, which allows the coupling behavior of axons to be related to the fiber-matrix interaction parameter, ϕ .

2. Model Development

Transversely isotropic hyperelastic model

Within the framework of continuum mechanics (Spencer 1984, Holzapfel 2000, Fung 2001, Volokh 2018) for the large deformation of an elastic body, the deformation gradient tensor is denoted as $F = \frac{\partial x}{\partial X}$, where X is a material vector in the reference configuration, and x is the corresponding deformed vector in the deformed configuration. The right and left Cauchy-Green tensors are $C = F^T F$ and $B = F F^T$, respectively. It is hypothesized that the strain energy density function for a transversely isotropic material can be written as a function of the invariants of the right Cauchy-Green tensor C,

$$\psi(\mathbf{C}) = \psi(I_1, I_2, I_3, I_4, I_5) \tag{1}$$

where $I_1 = tr(C)$, $I_2 = \frac{1}{2}\{[tr(C)]^2 - tr(C^2)\}$, $I_3 = det(C)$, $I_4 = a_0 \cdot Ca_0$, $I_5 = a_0 \cdot C^2a_0$ and a_0 is the unit vector along the mean fiber direction in the reference configuration. I_4 and I_5 are

pseudo-invariants under rotation about the axis of symmetry. The second Piola-Kirchhoff stress tensor can be obtained using the chain rule,

$$S = 2 \frac{\partial \psi(c)}{\partial c} = 2 \sum_{\alpha=1}^{5} \frac{\partial \psi(I_1, I_2, \dots, I_5)}{\partial I_{\alpha}} \frac{\partial I_{\alpha}}{\partial c}$$
 (2)

and subsequently implemented to derive the Cauchy stress as follows

$$\sigma = J^{-1} F S F^T \tag{3}$$

where $J = \det(F)$ is the Jacobian of the deformation gradient tensor.

Feng (2013) proposed a new strain energy density function accounting for the stretch ratio's contributions in the fiber direction as well as the contributions of shear strain in planes parallel to the fiber axis. The new strain energy density function is

$$\psi = \frac{\mu}{2} [(\bar{I}_1 - 3) + \zeta(\bar{I}_4 - 1)^2 + \phi \bar{I}_5^*] + \frac{\kappa}{2} (J - 1)^2$$
 (4)

where \bar{I}_1 and \bar{I}_4 are modified principal invariants of the modified right Cauchy-Green tensor $\bar{C} = \bar{F}^T \bar{F}$ and κ is the bulk modulus. The unimodular deformation gradient tensor is $\bar{F} = J^{-\frac{1}{3}} \bar{F}$. The shear strain in planes parallel to the fiber axis is denoted by a quadratic function, namely $\bar{I}_5^* = \bar{I}_5 - \bar{I}_4^2$, when the fiber axis is X_1 is considered. Similarly, \bar{I}_5 is a modified principal invariant of the modified right Cauchy-Green tensor \bar{C} . Following a tensorial operation procedure highlighted in Eqs (1-4), the Cauchy stress can be obtained as

$$\boldsymbol{\sigma} = \mu J^{-1} \overline{\boldsymbol{B}} + \left\{ \kappa (J - 1) - 2\mu J^{-1} \left[\frac{1}{6} \overline{I}_1 + \frac{\zeta}{3} \overline{I}_4 (\overline{I}_4 - 1) + \frac{\phi}{3} \overline{I}_5^* \right] \right\} \mathbf{I} + 2\mu J^{-1} [\zeta (\overline{I}_4 - 1) - \phi \overline{I}_4] \overline{\boldsymbol{a}} \otimes \overline{\boldsymbol{a}} + \mu \phi J^{-1} (\overline{\boldsymbol{a}} \otimes \overline{\boldsymbol{B}} \overline{\boldsymbol{a}} + \overline{\boldsymbol{B}} \overline{\boldsymbol{a}} \otimes \overline{\boldsymbol{a}})$$
 (5)

where $\overline{a} = \overline{F}a_0$. A detailed derivation of the constitutive equation can be found in Appendix A following a similar procedure to Feng (2013). Equation (5) is a four-parameter constitutive equation for reinforced materials that demonstrate transversely hyperelastic behavior, such as the

CNS white matter. This formulation should be solved according to the desired loading conditions to develop stress-strain laws for each testing mode.

Simple Shear in the Transversely Isotropic Plane

There are generally four parameters in the transversely isotropic hyperelastic constitutive relation of Eq. (5). For an incompressible material that corresponds to J-1=0 parameter κ may be regarded as a Lagrangian multiplier, and it should be obtained from the solution of equilibrium equations of motion using appropriate boundary conditions (Spencer 1984, Volokh 2018). Furthermore, three simple loading cases are consecutively considered to determine the other three material parameters μ , ϕ , and ζ . The axon direction α_0 is assumed to be along the X_1 axis. The first loading case is in-plane simple shear in the transverse isotropic plane. The deformation is described by

$$x_1 = X_1, \ x_2 = X_2 + \gamma_{23} X_3, \ x_3 = X_3 \tag{6}$$

thus, the deformation gradient is expressed by

$$\mathbf{F} = \frac{\partial x}{\partial \mathbf{X}} = \begin{bmatrix} 1 & 0 & 0 \\ 0 & 1 & \gamma_{23} \\ 0 & 0 & 1 \end{bmatrix} \tag{7}$$

while the modified right and left Cauchy-Green tensors are

$$\overline{C} = \overline{F}^T \overline{F} = \begin{bmatrix} 1 & 0 & 0 \\ 0 & 1 & \gamma_{23} \\ 0 & \gamma_{23} & 1 + \gamma_{23}^2 \end{bmatrix}$$
(8)

and,

$$\bar{\mathbf{B}} = \bar{\mathbf{F}}^T \bar{\mathbf{F}} = \begin{bmatrix} 1 & 0 & 0 \\ 0 & 1 & \gamma_{23} \\ 0 & \gamma_{23} & 1 + \gamma_{23}^2 \end{bmatrix}$$
(9)

In the undeformed space, the axon direction $oldsymbol{a_0}$ is described by

$$\boldsymbol{a_0} = \begin{bmatrix} 1 \\ 0 \\ 0 \end{bmatrix} \tag{10}$$

and, in the transformed space, by

$$\overline{a} = J^{-\frac{1}{3}} a = J^{-\frac{1}{3}} F a_0. \tag{11}$$

From the right Cauchy-Green tensor \overline{C} , it is straightforward to get the invariants $\overline{I}_1 = 3 + \gamma_{23}^2$, $\overline{I}_4 = 1$, $\overline{I}_5^* = 0$. Substitution into Eq. (5) results in the in-plane shear stress σ_{23} that is expressed in terms of the γ_{23} shear strain as

$$\sigma_{23} = \mu \gamma_{23}. \tag{12}$$

The above equiation implies that parameter μ is the in-plane shear modulus.

Simple Shear in the Anisotropic Plane

A simple shear can be applied in a plane parallel to the axon direction to measure the second parameter ϕ . This process is initiated by denoting the loading conditions as

$$x_1 = X_1 + \gamma_{12} X_2, \ x_2 = X_2, \ x_3 = X_3 \tag{13}$$

and by following a similar procedure as above, the simple stress-strain relation can be written as

$$\sigma_{12} = \mu(1+\phi)\gamma_{12}.\tag{14}$$

The introduction of the parameter, ϕ , to the relation implies in-plane coupling of the axons. Since the in-plane shear parameter μ has been determined previously, the coupling parameter ϕ can be determined using Eq. (14).

Uniaxial Tension

The last parameter ζ , is determined by a simple uniaxial tensile test assuming a stretch ratio λ_1 in the X_1 direction. For an incompressible material, the deformation can be written as,

$$x_1 = \lambda_1 X_1, \ x_2 = \lambda_1^{-\frac{1}{2}} X_2, \ x_3 = \lambda_1^{-\frac{1}{2}} X_3$$
 (15)

The deformation gradient tensor is therefore expressed by,

$$\mathbf{F} = \frac{\partial x}{\partial x} = \begin{bmatrix} \lambda_1 & 0 & 0 \\ 0 & \lambda_1^{-\frac{1}{2}} & 0 \\ 0 & 0 & \lambda_1^{-\frac{1}{2}} \end{bmatrix}. \tag{16}$$

The above relation automatically satisfies the incompressibility condition $det(\mathbf{F}) = 1$. Following a similar procedure using Eq. (5), one can derive

$$\sigma_{11} = \mu(\lambda_1^2 - \lambda_1^{-1}) + 2\mu\zeta\lambda_1^2(\lambda_1^2 - 1). \tag{17}$$

During the derivation of Eq. (17) the condition of $\sigma_{22} = \sigma_{33} = 0$ is enforced in accordance to uniaxial tension testing. Since the in-plane shear modulus μ has been determined using Eq. (12), the fiber contribution parameter ζ can be obtained using uniaxial stress-stretch relation.

Parameter Determination

Once the experimental data is available for all three of these testing modes, it is straightforward to determine the parameters μ , ϕ , and ζ of the strain energy density function by using Eqs. (12), (14), and (17). However, it is usually difficult to perform all three different tests on soft tissues due to practical difficulties such as sample preparation and sample gripping (Miller 2000). New experimental techniques such as dynamic tests (Okamoto 2011, Rashid 2012a, Rashid 2014) and indentation tests (van Dommelen 2010, Namani 2012) have been developed to estimate the material properties. For some of these non-trivial tests, finite element analysis has been combined with the test to estimate material parameters (Ho 2007, Rashid 2012b, Feng 2013, Javid 2014). Moreover, finite element analysis is a robust approach for studying the behavior of soft biological tissues ranging from microscopic to macroscopic scales (Karami 2009, Pan 2011, Pindera 2013,

Pan 2013, Karami 2013, Labus 2016). In this study, where axon tortuosity and kinematic coupling is included, in addition to white matter anisotropy, only uniaxial tension data is available. As a result, these data are combined with virtual data extracted from a simulation of white matter RVEs executed in the shear modes.

3. Test and Modeling Results

Uniaxial test data are taken from an experimental study of the influence of myelin and glia on the mechanical behavior of chick embryo spinal cord following disruption of the glial matrix in ovo using either Ethidium Bromide (EB) or an antibody against galactocerebroside (α GalC) (Shreiber 2009). These data are especially valuable because they provide test cases of the same tissue with different kinematic coupling degrees. Ethidium Bromide is cytotoxic to dividing cells and thereby disrupts the glial matrix by killing astrocytes and oligodendrocytes. Conversely, α GalC interferes with the development of myelination, and thereby disrupts the glial matrix with substantial cytotoxic effects. Spinal cords demyelinated with either approach demonstrate significantly lower stiffness and ultimate tensile stress than myelinated spinal cords. The results demonstrate that the glial matrix provides significant mechanical support to the spinal cord, and suggests that myelin and cellular coupling of axons via the glial matrix in large part dictates the tensile response of the tissue.

The nonlinear uniaxial tensile data are used as one loading case. To fully determine the parameters of the transversely hyperelastic model for white matter, two shear load simulations are performed on the RVE of the chick embryo spinal cord to generate virtual stress-strain data. The RVE is composed of a 0.4 μ m x 10 μ m x 5.68 μ m cubic region representing the extracellular matrix and 33 axons whose tortuosity ranging from 1.05 to 1.25. The volume fraction of the axon

in the RVE is 53%. A detailed description of the development and testing of the RVE can be found in Pan et al. (2013), where the effect of the transition from non-affine to affine interactions of axons and matrix during uniaxial tensile loading of the spinal cord was investigated. This model is employed here to generated virtual stress-strain data for the in-plane and out-of-plane shear loadings at three, 0%, 25%, and 50%, axon and ECM fixed coupling levels. EB-treated tissue is assumed purely uncoupled; thus, the interaction between the axon and the ECM matrix is set to 0%, representing non-affine kinematics between the axon and the ECM. Untreated tissue where the coupling level is not known, interaction levels of 25% and 50% are considered for control. To enable the computational interaction between the axons and the ECM the corresponding percentage of the axonal surface area is tied to the surrounding ECM while the rest of the axonal surface remains is united. Furthermore, soft brain tissue consists of a high percentage of water thus exhibiting a rubber-like material response under mechanical loading. That led many researchers to use Ogden's hyperelastic model to simulate its mechannical behavior (Shreiber 2009, Rashid 2012a, 2012b, Labus 2016). Here, the axons and ECM are both treated as isotropic materials, and the Ogden's isotropic hyperelastic material model is employed in its strain energy form (Hao and Shreiber 2007)

$$W = \frac{2G}{\alpha^2} \left(\lambda_1^{\alpha} + \lambda_2^{\alpha} + \lambda_2^{\alpha} - 3 \right) \tag{18}$$

where G represents the shear modulus, α is a material-dependent parameter that introduces non-linear behavior, and λ_i are the principal stretches. The nonlinear material parameters α and G of the glial matrix are taken from Ethidium Bromide treated chick spinal cord test data (Shreiber 2009), while each axon is considered as transversely isotropic. Due to the lack of data and for simplicity, the Ogden's isotropic hyperelastic model is employed similarly to the Arbogast (1999) and Meaney (2003) studies where the shear modulus of an axon is assumed to be three times stiffer

than that of the ECM. The parameters are provided in Table 1, and they are of the same order of magnitude as the parameters reported for porcine brains using the same Ogden model (Rashid 2014).

Displacement boundary conditions are applied to the RVE to simulate the two simple shear tests, and the average reaction stresses are recorded. The first simple shear test is within the transverse $X_2 - X_3$ plane, as shown in Fig. 2(a). The second simple shear test is within the $X_1 - X_2$ plane, as shown in Fig. 2(b). The virtual shear stress-strain curves, are plotted in Figs 3-5 where the effect of the three levels of axon/matrix coupling, 0%, 25%, and 50%, is captured.

Two approaches may be considered for the determination of the constitutive parameters μ , ϕ and ζ . The first approach considers only one parameter, i.e., shear modulus, μ , in Eq. (12), whose values are determined by a simple computational shear test in the plane transverse to the axons (inset in Fig. 2(a)). Once the shear modulus μ is determined, the data from the in-plane shear test can be used to fit Eq. (14) and determine the parameter ϕ , and data from uniaxial testing can be used to fit Eq. (17) to find the parameter ζ . The second approach, which is used in our analysis, employs a least-squares method and fits Eq. (12), Eq. (14), and Eq. (17) simultaneously to determine μ , ϕ , and ζ . This implementation avoids biasing the analysis towards any of the testing modes. It should be noted that there might be multiple solutions (local minima) when solving the optimization problem of curve-fitting of hyperelastic models (Ogden 2004) whose parametric equations are nonlinear. Since our model defined by Eqs (12, 14 & 17) is decoupled, the parameters are unique.

Interpretation of data is performed by fitting the error of each parameter is computed and added to the table. The results were split into two groups to avoid confusion stemming from the comparison between the treated test assuming 0% interaction and the control test, assuming 25%

or 50% interaction. One set representing the 0% and 25% interaction level cases (Table 2a) and an additional set representing the 0% and 50% interaction level cases (Table 2b) is pursued to test the model's capabilities further.

As described above, two sets of experimental uniaxial tension stress-strain data are available to tease out the role of axon-matrix coupling on parameter determination for the bulk mechanical response of white matter. EB-treated, demyelinated chick spinal cords are considered fully uncoupled at the microstructural level, and 0% interaction between axons and matrix is prescribed for the RVE model to simulate the response in shear. These two groups of shear data are referred to as numerical test data. The comparison of model predictions and the test data is illustrated in Fig. 3, and parameter results are listed in Table 2(a-b). The axon-matrix interaction is 0%; thus, the shear modulus ($\mu = 17.1$ kPa) in the transverse plane of the white matter is close to the shear modulus of the matrix in the RVE model (G = 17.4 kPa).

The level of interaction between the axons and the ECM for the control chick spinal cord is undetermined, and either 25% or 50% interaction simulation data (simple shear) were combined with the control uniaxial tensile test data to fit for the parameters. The fitted curves and model prediction for 25% and 50% level of interaction are plotted in Figs 4 and 5, respectively. The parameters are also reported in Table 2.

As noted in Eq. (12) the parameter μ represents the shear modulus of the composite in the material plane perpendicular to the axon direction. Note that as the value of μ increases as the level of interaction between the axon and the ECM increases. From Eq. (14), it is apparent that ϕ is a parameter measuring the non-dimensional relative shear anisotropy. The axon-ECM coupling driven shear anisotropy is demonstrated when comparing the left plot of Figs 3, 4, and 5. If we examine the strain energy function, it corresponds to the strain energy contributed by the fiber

deformation other than stretching. The third parameter, ζ , represents the non-dimensional stretch anisotropy. The fitted curves deviate from the experimental curves in the uniaxial tensile test, where the third parameter is involved. It is noted that the fitted curve is much stiffer at lower stretches than the experimental data. The latter may be due to the lower axon contribution at lower stretch levels in the model, whereas a stretch-dependent transition from non-affine to affine kinematics is observed (Bain 2003, Hao 2007). Here, there is a constant interaction at 25% or 50% of the axons throughout the simulation, instead of an interaction level transitioning from low to high gradually as more axons are engaged during the stretching process (Pan 2011 and 2013). Therefore, to capture the transitional coupling of axons and ECM more accurately, a stretch-dependent coupling parameter may be required in a future study.

Summarily in Figs 3-5, the parameters μ and ϕ are increasing, while the parameter ζ is decreasing. One should note that ϕ represents the relative shear anisotropy. When the interaction between axon and ECM is 0%, the axon contribution is minimal, and the fitting error is of the same magnitude of the parameter. As seen, the parameter ϕ increases as the level of interaction increases. Nevertheless, it is hard to discern which group (0% - 25% or 0% - 50%) is close to the realistic situation. The fact that the prediction increases from the treated to the control is satisfactory and agrees with reported data in Shreiber 2016. While this proof is within the scope of the presented work, future efforts will focus on identifying predicted or fitted interaction percentages that reflect real interaction percentages.

4. Discussion and Conclusions

In this paper, a hybrid method comprised of experimental and computational tests is studied in the context of its effectiveness to capture the hyperelastic response of white matter tissue in loading cases where testing data is unattainable. Experimental data from uniaxial tension is combined with a finite element model built from the microstructure of axons and their interaction with the surrounding ECM to determine the macroscopic material constitutive law parameters. Feng's (2013) transversely isotropic hyperelastic model that accounts for the axon-ECM contribution to the strain energy density function is selected, and it is proven capable of representing some tissues in which axons are highly organized and relatively straight in the corpus callosum. When applied to the chick embryo spinal cord data of this study, there is some discrepancy between the uniaxial tension test stretch-stress data and the fitted curves. The model prediction shows a stiffer response as compared to the experimental data at a low stretch ($\lambda < 1.2$). It implies that the model lacks the mechanism of describing the transitional kinematics of axons in the chick embryo spinal cord. To this end, the interaction between the axon and the extracellular matrix may be affine since the axons are highly organized and relatively straight in the corpus callosum (Johnson 2013). In the limiting case where axons and matrix are fully uncoupled, the macroscale parameter μ (macroscale shear modulus) and the microscale shear modulus are in agreement, and the parameter ϕ , which introduces coupling in the plane parallel to the axons (relative shear anisotropy), is close to zero. When coupling at the microscale is introduced, the macroscale coupling parameter, ϕ , increases, while the stretch anisotropy, ζ , decreases. Interestingly, these two parameters appear to balance the ultimate effects on the macroscale shear modulus, μ . A composite model that recruits the noneaffine kinematics is yet to be developed for tissues with highly undulated fibers such as chick
embryo spinal cord and cerebral of the brain. Nonetheless, a hybrid approach that combines finite
element virtual tests, based on the microarchitecture and micromechanics of the axon-ECM
interaction, and experimental data is demonstrated. Material parameters can then be determined
using the hybrid data to model large deformation, transversely isotropic behavior of white matter.
This model is expected to simplify significantly multi-scale modeling efforts by allowing a "closed
form" estimate of material properties at the tissue level. Finally, the presented hybrid approach
enables the validation of tissue models when the microscale architecture prohibits in-situ
experimentation. This validation is accomplished by regressively employing hybrid data from
existing experiments in conjunction with virtual, numerical tests.

Acknowledgements

The authors gratefully acknowledge the support of the New Jersey Commission on Spinal Cord Research (CSCR17ERG010), and the National Science Foundation (NSF CMMI Grants #1436743 and #1762774).

References

- Armstrong, B.C., Ruiz-Blondet, M., Khalifian, N., Kurt, K.J., Jin, Z., and Laszlo, S. (2015). Brainprint: Assessing the uniqueness, collectability, and permanence of a novel method for ERP biometrics. Neurocomputing, 166, 59-67. http://dx.doi.org/10.1016/j.neucom.2015.04.02.
- Arbogast, K.B. and Margulies, S.S. (1999). A fiber-reinforced composite model of the viscoelastic behavior of the brainstem in shear. Journal of Biomechanics 32:865-870.
- Bain, A.C., Shreiber, D.I. and Meaney, D.F. (2003). Modeling of microstructural kinematics during simple elongation of central nervous system tissue. Transactions of the ASME. 125:798-804.
- Carlsen R. W., Daphalapurkar N. P. (2015) The Importance of Structural Anisotropy in Computational Models of Traumatic Brain Injury, Front Neurol. 2015; 6:28.
- Faul, M., Xu, L., Wald, M. M., Coronado, V.G., (2010) Traumatic Brain Injury in the United States: Emergency Department Visits, Hospitalizations and Deaths 2002–2006, http://www.cdc.gov/traumaticbraininjury/pdf/blue book.pdf.
- Feng, Y, Okamotoa, R. J., Namania, R., Genina, G. M., Bayly, P. V., (2013) Measurements of mechanical anisotropy in brain tissue and implications for transversely isotropic material models of white matter. Journal of the mechanical behavior of biomedical materials 23:117–132.
- Fung, Y.C and Tong, P. (2001) Classical and Computational Solid Mechanics, Advanced Series in Engineering Science Vol. 1, World Scientific.
- Gasser, T.C., Ogden, R.W., and Holzapfel, G.A., (2006) Hyperelastic modeling of arterial layers with distributed collagen fiber orientations, J. R. Soc. Interface, 3:15–35.

- Giordano, C., Kleiven, S., (2014) Connecting fractional anisotropy from medical images with mechanical anisotropy of a hyperviscoelastic fibre-reinforced constitutive model for brain tissue.

 J. R. Soc. Interface 11(91):20130914. doi: 10.1098/rsif.2013.0914
- Goriely, A., Geers, M.G.D., Holzapfel, G.A., Jayamohan, J., Jerusalem, A., Sivaloganathan, S., Squier, W., van Sommelen, J.A.W., Waters, S., and Kuhl, E., (2015), Mechanics of the brain: perspectives, challenges, and opportunities. Biomechanics and Modeling in Mechanobiology 14:931–965.
- Hao, H., and Shreiber, D.I., (2007) Axon kinematics change during growth and development, Journal of Biomechanical Engineering, vol. 129.
- Ho, J. and Kleiven S. (2007). Dynamic response of the brain with vasculature: A three-dimensional computational study, *J. Biomech.* 40:3006–3012.
- Holzapfel, G.A. (2000). Nonlinear Solid Mechanics: A Continuum Approach for Engineering, Wiley, ISBN-13: 978-0471823193
- Javid, S., Rezaei, A., Karami, G., (2014) A micromechanical procedure for viscoelastic characterization of the axons and ECM of the brainstem, Journal of the Mechanical Behavior of Biomedical Materials, 30:290-299.
- Johnson, C.L., McGarry, M.D.J., Gharibans, A.A., Weaver, J.B., Paulsen, K.D., Wang H., Olivero, W.C., Sutton, B.P., and Georgiadis, J.G., (2013) Local mechanical properties of white matter structures in the human brain, NeuroImage, 79(1):145-152.
- Kakulas, B. A., (1999) A Review of the Neuropathology of Human Spinal Cord Injury With Emphasis on Special Features, J. Spinal Cord Med., 22(2):119–124.

- Karami, G., Grundman, N., Abolfathi, N., Naik, A., and Ziejewski, M., J. (2009). A micromechanical hyperelastic modeling of brain white matter under large deformation. J. Mech. Behav.of Biomed.Mate. 2:243-254.
- Labus, K.M., Puttlitz, C.M., (2016) An anisotropic hyperelastic constitutive model of brain white matter in biaxial tension and structural—mechanical relation-ships. J. Mech. Behav. Biomed. 62: 195–208.
- Meaney, D.F., (2003) Relationship between structural modeling and hyperelastic material behavior: application to CNS white matter, Biomechanics and Modeling in Mechanobiology, 1:279-293.
- Miller, K., Chinzei, K., Orssengo, G., and Bednarz, P., (2000) Mechanical properties of brain tissue in-vivo: experiment and computer simulation. Journal of Biomechanics, 33: 1369-1376.
- Namani, R., Feng, Y., Okamoto, R.J., Jesuraj, N., Sakiyama-Elbert, S.E., Genin, G.M., Bayly, P.V., (2012), Elastic characterization of transversely isotropics of materials by dynamic shear and asymmetric indentation. Journal of Biomechanical Engineering 134 (6):061004.
- Ogden, R.W. (1972), Large deformation isotropic elasticity II: On the correlation of theory and experiment for incompressible rubber like solids. Proceedings of the Royal Society A 326, 565-584
- Ogden, R.W., Saccomandi, G., and Sgura, I., (2004) Fitting hyperelastic models to experimental data. Computational Mechanics 34:484-502.

- Okamoto, R.J., Clayton, E.H., Bayly, P.V., (2011) Viscoelastic properties of soft gels: comparison of magnetic resonance elastography and dynamic shear testing in the shear wave regime. Physics in Medicine & Biology 56:6379–6400.
- Pan, Y., Shreiber, D.I., and Pelegri, A.A., (2011) A Transition Model for Finite Element Simulation of Kinematics of Central Nervous System White Matter, IEEE Transactions on Biomedical Engineering, 58(12):3443-6.
- Pan, Y., Sullivan, Shreiber, D.I., and Pelegri, A.A., (2013) Finite element modeling of CNS white matter kinematics: use of a 3D RVE to determine material properties, Frontiers in Bioengineering and Biotechnology, 1. doi.org/10.3389/fbioe.2013.00019
- Rashid B., Destrade M., Gilchrist M.D. (2012a) Mechanical characterization of brain tissue in compression at dynamic strain rates, Journal of the Mechanical Behavior of Biomedical Materials, 10:23-38.
- Rashid B., Destrade M., Gilchrist M.D. (2012b) Inhomogeneous deformation of brain tissue during tension tests, Computational Materials ScienceVolume 64:295-300
- Rashid B., Destrade M., Gilchrist, M.D., (2014) Mechanical characterization of brain tissue in tension at dynamic strain rates, Journal of the Mechanical Behavior of Biomedical Materials, 33:43-54
- Spencer, A.J.M., (1984) Constitutive Theory for Strongerly Anisotropic Solids, in Continuum Theory of the Mechanics of Fibre-Reinforced Composites. Edited by A.J.M. Spencer.

Shreiber, D.I., Hao,H., and Elias, R.A. (2009). Probing the influence of myelin and glia on the tensile properties of the spinal cord. Biomechanics and Modeling in Mechanobiology. 8:311–321.

Tu, W., Pindera, M.J., (2013) Targeting the finite-deformation response of wavy biological tissues with bio-inspired material architectures, Journal of the Mechanical Behavior of Biomedical Materials, 28:291-308

van Dommelen, J.A.W., van der Sande, T.P.J., Hrapko, M., Peters, G.W.M., (2010) Mechanical properties of brain tissue by indentation: Interregional variation, Journal of the Mechanical Behavior of Biomedical Materials, 3(2):158-166.

Volokh K., (2018) Mechanics of Soft Materials, ISBN-13: 9789811093968, Springer Singapore.

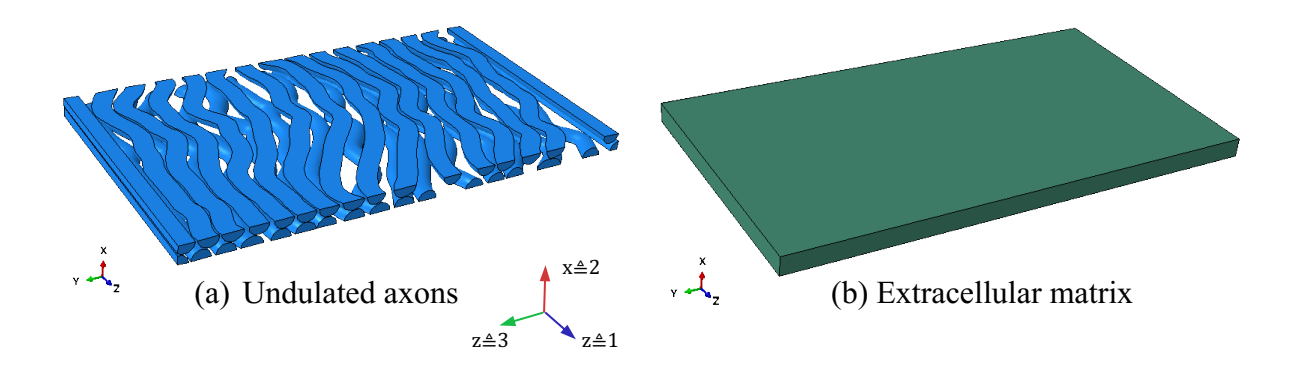


Figure 1. Finite element model of the (a) undulated axons, and (b) extracellular matrix.

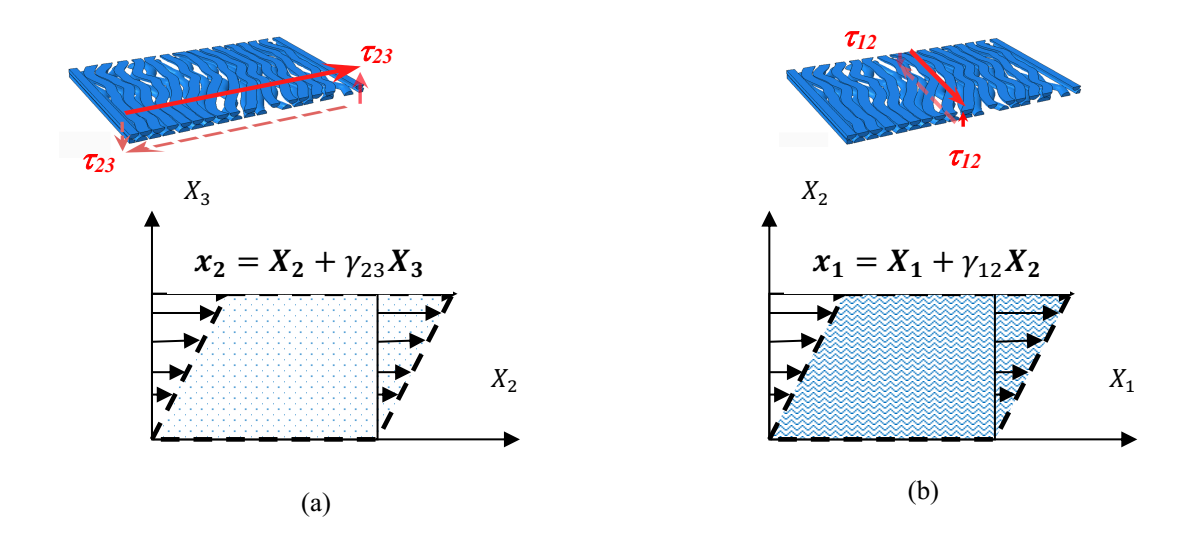


Figure 2. (a) Shear test in the 23-plane transverse to the major axon direction, and (b) shear test in the 12-plane parallel to the major axon direction

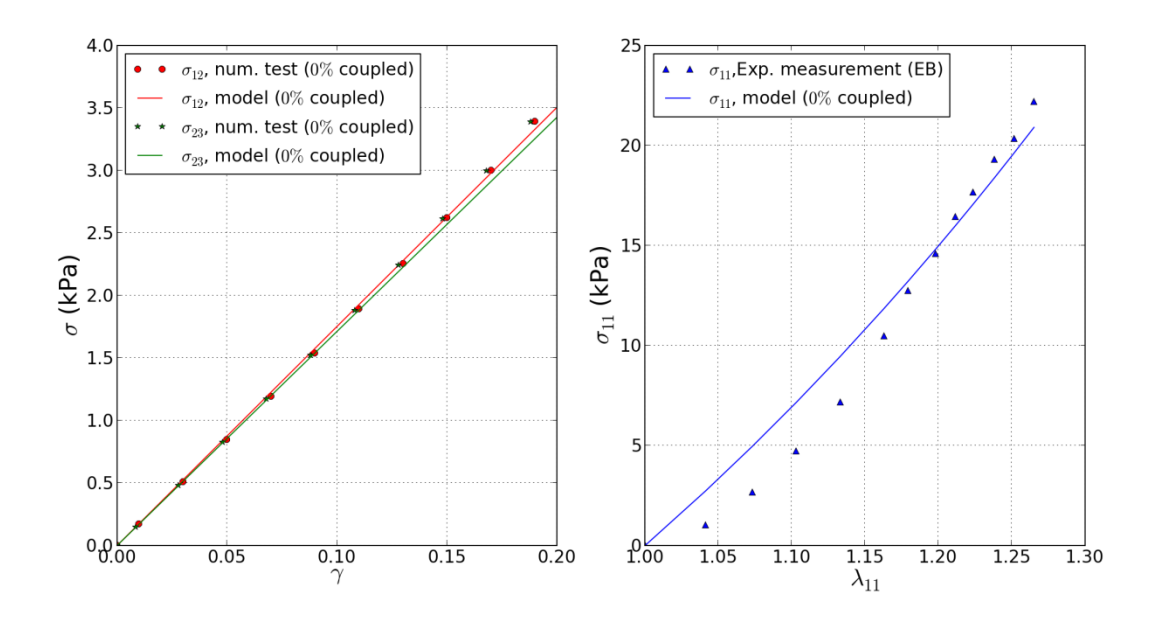


Figure 3. Comparison of virtual stress-strain data from the finite element simulation of the RVE (*Left*) or uniaxial tension data (*Right*) to the best fit macroscale response for uncoupled tissue.

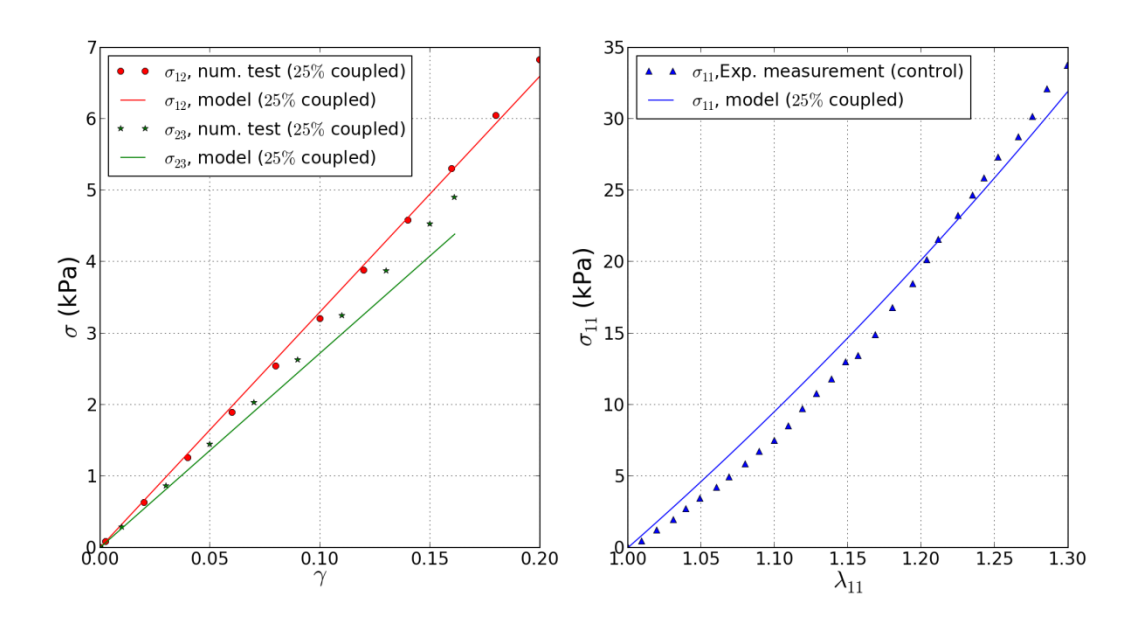


Figure 4. Comparison of virtual stress-strain data from the finite element simulation of the RVE (*Left*) or uniaxial tension data (*Right*) to the best fit macroscale response for tissue that is coupled 25% at the microscale.

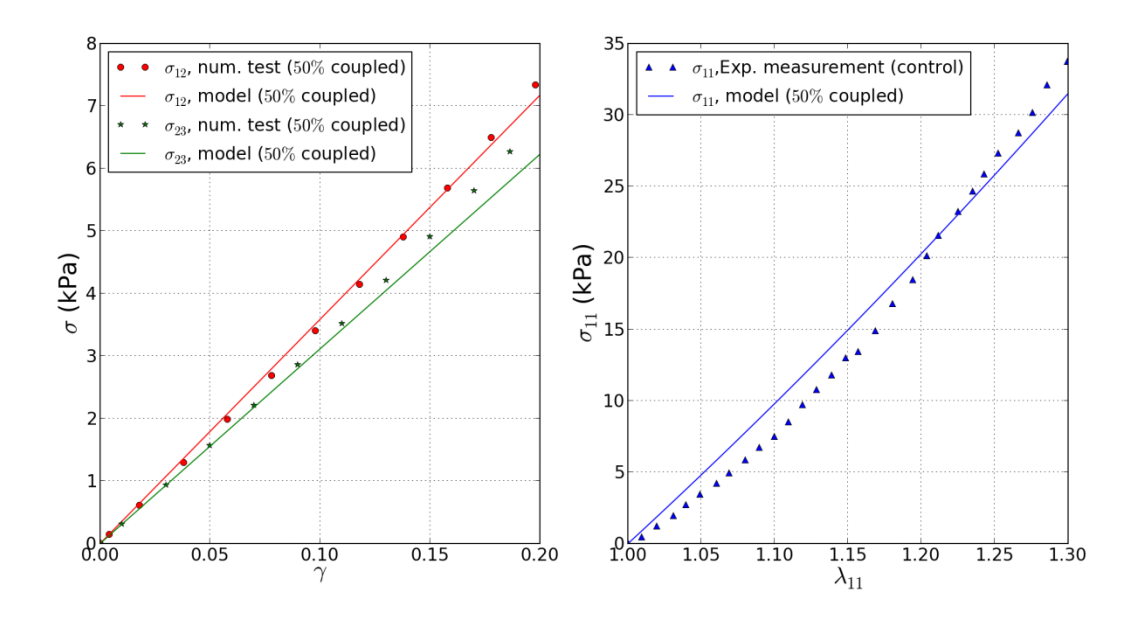


Figure 5 Comparison of virtual stress-strain data from the finite element simulation of the RVE (*Left*) or uniaxial tension data (*Right*) to the best fit macroscale response for tissue that is coupled 50% at the microscale.

Table 1: Parameters of Ogden model for the constituents in the microscale RVE model

Ogden Parameters	ECM	Axon
G (kPa)	17.4	52.2
α	8.32	8.32

Table 2 a: Best fit parameters for the macroscale strain energy function at different levels of microscale axon-to-matrix coupling. Absolute fitting error is listed in the bracket using the python scipy.optimize.leastsq function.

Coupling level	0%	25%
μ (kPa)	17.1 (0.3)	27.2 (0.5)
φ	0.023	0.212 (0.029)
ζ	0.185	0.079 (0.012)

Table 2 b: Best fit parameters for the macroscale strain energy function at different levels of microscale axon-to-matrix coupling.

Coupling level	0%	50%
μ (kPa)	17.1 (0.3)	31.1 (0.5)
1	0.023	0.153 (0.033)
φ	(0.023)	0.152 (0.023)
ζ	0.185	2 222 (2 227)
	(0.013)	0.009 (0.007)

Appendix A

Kinematics of large deformation

Consider a body which deforms from a volume V in the undeformed configuration R_o in to a volume v in the deformed configuration R. The motion of the body is described by the relation

$$\mathbf{x} = \mathbf{x}(\mathbf{X}, t) \tag{1}$$

where t is time, and x represents the position of a point in R associated with a material point originally located at X in R_o . The deformation gradient tensor is defined as

$$F = \frac{\partial x}{\partial x} \tag{2}$$

The Jacobian is denoted as J = det(F), representing the ratio of deformed to undeformed volumes. The right Cauchy-Green tensor and left Cauchy-Green tensor are $C = F^T F$ and $B = FF^T$. The Green strain tensor is $E = \frac{1}{2}(C - I)$.

The deformation gradient tensor is multiplicatively decomposed to volumetric and distortional parts.

$$F = J^{\frac{1}{3}}\overline{F} \tag{3}$$

where $\overline{F} = J^{-\frac{1}{3}} F$ is the isochoric or distortional part of deformation that preserves volume, i.e.,

$$det(\overline{F}) = 1 \tag{4}$$

The modified right Cauchy-Green tensor and left Cauchy-Green tensor are $\overline{C} = \overline{F}^T \overline{F}$ and $\overline{B} = \overline{F} \overline{F}^T$. For a transversely isotropic hyperelastic with fiber direction in a_0 , one might decompose the strain energy density function into a volumetric part and a distortional (or isochoric) part as

$$\psi = U(J) + \bar{\psi}(\overline{C}, a_0) \tag{5}$$

Feng (2013) proposed a volumetric function to describe the volumetric component of the strain energy, U(J), as

$$U(J) = \frac{\kappa}{2}(J-1)^2,$$
 (6)

where k is the bulk modulus. He then decomposed the isochoric strain energy density function into a neo-Hookean function and a function accounting for anisotropy as

$$\overline{\psi}(\overline{C}, a_0) = \frac{\mu}{2} [(\overline{I}_1 - 3) + \zeta(\overline{I}_4 - 1)^2 + \phi \overline{I}_5^*]$$
 (7)

where,

$$\bar{I}_1 = tr(\overline{C}), \bar{I}_4 = a_0 \cdot \overline{C}a_0, \ \bar{I}_5 = a_0 \cdot \overline{C}^2a_0 \text{ and } \bar{I}_5^* = \bar{I}_5 - \bar{I}_4^2.$$
 (8)

The fiber direction in the deformed configuration is $a = Fa_0$. The 2nd Piola-Kirchhoff stress is

$$S = S_{vol} + \overline{S} \tag{9}$$

where,

$$\mathbf{S}_{vol} = \frac{\partial U(J)}{\partial E} = 2 \frac{\partial U(J)}{\partial C} = \kappa (J - 1) J \mathbf{C}^{-1}$$
 (10)

$$\overline{S} = 2 \frac{\partial \overline{\psi}(\overline{c}, a_0)}{\partial c} = 2 \frac{\partial \overline{\psi}(\overline{c}, a_0)}{\partial \overline{c}} \frac{\partial \overline{c}}{\partial c}$$
(11)

It is straight forward to show that,

$$\frac{\partial \overline{c}}{\partial c} = J^{-\frac{2}{3}} (\mathbb{I} - \frac{1}{3} \overline{C} \otimes \overline{C}^{-1}), \tag{12}$$

where I denotes the fourth-order identity tensor, which has the form

$$(\mathbb{I})_{ijkl} = \frac{\delta_{ik}\delta_{jl} + \delta_{il}\delta_{jk}}{2},\tag{13}$$

with δ_{ik} being the Kronecker delta.

Substitute(12) into (11), and then substitute (10) and (11) into (9) to get,

$$S = \kappa (J-1)JC^{-1} + 2J^{-\frac{2}{3}}Dev(\frac{\partial \bar{\psi}}{\partial \bar{c}})$$
 (14)

where $\mathbf{Dev}()$ is an operator, $\mathbf{Dev}(*) = (*) - \frac{1}{3}[(*):\overline{\mathbf{C}}]\overline{\mathbf{C}}^{-1}$.

Apply a push forward for (14) to get the Cauchy stress tensor

$$\boldsymbol{\sigma} = J^{-1} \boldsymbol{F} \boldsymbol{S} \boldsymbol{F}^T \tag{15}$$

Substitute (14) into (15) and simply, the Cauchy stress is then

$$\boldsymbol{\sigma} = \kappa (J-1)\boldsymbol{I} + 2J^{-1}dev(\overline{\boldsymbol{F}}\frac{\partial \overline{\psi}}{\partial \overline{c}}\overline{\boldsymbol{F}}^T)$$
 (16)

where dev() is a tensorial operator, $dev(*) = (*) - \frac{1}{3}[(*):I]I$. This operator enables the deviatoric nature of a second-order tensor Z such that dev(Z):I=0.

Using the chain rule of derivative,

$$\frac{\partial \bar{\psi}}{\partial \bar{c}} = \frac{\partial \bar{\psi}}{\partial \bar{I}_1} \frac{\partial \bar{I}_1}{\partial \bar{c}} + \frac{\partial \bar{\psi}}{\partial \bar{I}_4} \frac{\partial \bar{I}_4}{\partial \bar{c}} + \frac{\partial \bar{\psi}}{\partial \bar{I}_5^*} \frac{\partial \bar{I}_5^*}{\partial \bar{c}}$$

$$\tag{17}$$

and substituting (17) into (16), and following some tensor operations, one will have a 4-parameter constitutive equation for incompressible hyperelastic materials,

$$\boldsymbol{\sigma} = \mu J^{-1} \overline{\boldsymbol{B}} + \left\{ \kappa (J - 1) - 2\mu J^{-1} \left[\frac{1}{6} \overline{I}_1 + \frac{\zeta}{3} \overline{I}_4 (\overline{I}_4 - 1) + \frac{\phi}{3} \overline{I}_5^* \right] \right\} \mathbf{I} + 2\mu J^{-1} [\zeta (\overline{I}_4 - 1) - \phi \overline{I}_4] \overline{\boldsymbol{a}} \otimes \overline{\boldsymbol{a}} + \mu \phi J^{-1} (\overline{\boldsymbol{a}} \otimes \overline{\boldsymbol{B}} \overline{\boldsymbol{a}} + \overline{\boldsymbol{B}} \overline{\boldsymbol{a}} \otimes \overline{\boldsymbol{a}}$$
(18)

where $\overline{a} = J^{-\frac{1}{3}}a$.